STATISTICS, OPTIMIZATION AND INFORMATION COMPUTING
Stat., Optim. Inf. Comput., Vol. **x**, Month 202x, pp 0–14.
Published online in International Academic Press (www.IAPress.org)

Performance of Bayesian Kriging under Different Levels of Spatial Autocorrelation: A Simulation Study of Rainfall Interpolation

Suci Astutik [1,*], Evellin Dewi Lusiana [1], Rismania Hartanti Putri Yulianing Damayanti [1], Agus Yarcana [1], Nanda Aptana Irsyadul Bahy [2]

[1]*Department of Statistics, Faculty of Mathematics and Natural Sciences, Universitas Brawijaya, Indonesia*
[2]*Department of Mechanical and Industrial Engineering, Universitas Gadjah Mada, Indonesia*

Abstract This study investigates the influence of spatial autocorrelation on the performance of Bayesian kriging for interpolating daily rainfall in East Java, Indonesia, using both empirical observation data and controlled simulation experiments. Daily rainfall records from multiple monitoring stations were analyzed to assess spatial dependence via Global Moran's I, revealing that the onset phase of the rainy season exhibits moderate to strong positive spatial autocorrelation, whereas the peak phase shows weak or negligible spatial structure dominated by local-scale variability. Cross-validation results indicate that stronger spatial autocorrelation significantly improves Bayesian kriging performance, as evidenced by lower RMSE and MAE. Simulation results further corroborate that Bayesian kriging yields substantial predictive gains when Moran's I exceeds approximately 0.30–0.40, while predictive improvement is marginal when Moran's I falls below 0.20. Under weak spatial dependence, the model effectively reduces to a nugget-driven process, that is, a process with minimal spatial continuity. These findings underscore that the effectiveness of Bayesian kriging for daily rainfall interpolation is fundamentally contingent upon the magnitude of spatial autocorrelation, highlighting the necessity of preliminary spatial diagnostics to guide appropriate methodological choices in geostatistical applications.

Keywords Bayesian, Kriging, Rainfall, Spatial Interpolation, Spatial, Spatial Autocorrelation

AMS 2010 subject classifications 62C10, 62F15

DOI: 10.19139/soic-2310-5070-3615

1. Introduction

Rainfall constitutes one of the principal hydrometeorological variables that exerts a crucial influence on multiple societal and environmental domains, including water resource governance, flood and drought management, agricultural planning, and disaster risk mitigation frameworks [1]. The inherently heterogeneous and spatial distribution of rainfall necessitates the availability of high-resolution. Nevertheless, rainfall measurements are typically acquired from fixed observation stations, resulting in spatial data that are discrete, fragmented, and spatially sparse. This intrinsic limitation constrains the capacity to delineate continuous rainfall fields across broader regions. Consequently, the implementation of spatial interpolation techniques becomes indispensable to infer and reconstruct rainfall distributions at unobserved locations.

In spatial analysis, various interpolation methods have been developed to estimate the value of a variable at unobserved locations based on data at available observation points. In general, spatial interpolation methods can be grouped into two main approaches, namely deterministic methods and geostatistical methods [2]. Deterministic interpolation methods aim to construct an estimation surface based on the degree of similarity between observation

*Correspondence to: Suci Astutik (Email: suci_sp@ub.ac.id). Department of Statistics, Faculty of Mathematics and Sciences, Universitas Brawijaya, Veteran Road, Malang, Indonesia (65145).

ISSN 2310-5070 (online) ISSN 2311-004X (print)

points. For example, through distance weighting such as Inverse Distance Weighting (IDW) or based on the degree of surface smoothing, as in the radial basis functions and spline approaches [3]. Deterministic techniques directly utilize the values at surrounding data points without explicitly modeling spatial dependency structures [2]. Thus, the resulting estimates are highly dependent on the geometric configuration and proximity between observation points, and do not formally accommodate the underlying uncertainty components or spatial covariance structures.

Interpolation using geostatistical techniques is widely recognized as a highly reliable approach for estimating values at unsampled locations, as they rely on a weighted averaging scheme that explicitly incorporates spatial dependence among neighboring observations [4, 5]. In particular, kriging integrates the spatial correlation structure through covariance functions or variograms, enabling the production of estimates that are generally more precise and statistically coherent than those obtained from purely deterministic interpolation methods. A comparative study by [6] evaluated four deterministic approaches alongside five geostatistical techniques in the context of a Jurassic karst aquifer and a Quaternary alluvial aquifer. Their validation, based on eco-hydrogeological indicators, demonstrated that geostatistical methods generally outperformed deterministic alternatives. Nevertheless, kriging is not without limitations. Its implementation depends on the assumption of stationarity in variogram estimation and typically treats variogram parameters as known, even though they are themselves estimated and therefore subject to uncertainty [7]. Furthermore, the distribution of observed phenomena may deviate from symmetry or normality due to natural constraints, such as upper and/or lower bounds. The covariance structure must often be inferred from a restricted set of pre-specified theoretical models, which may not fully capture the complexity of the underlying spatial process.

Bayesian Kriging emerged as a methodological advancement of classical kriging by situating spatial prediction within a fully Bayesian statistical framework. In contrast to conventional approaches that regard covariance parameters such as the sill, range, and nugget as fixed after estimation, the Bayesian formulation treats these quantities as random variables characterized by prior distributions that are subsequently updated to posterior distributions in light of the observed data [8, 9, 10]. This hierarchical structure enables explicit representation and propagation of parameter uncertainty into the predictive distribution, thereby yielding a more rigorous and internally consistent assessment of uncertainty.

The implementation of Bayesian Kriging has been explored in numerous scientific disciplines, including radiological characterisation [11], soil science [12, 13, 14], ecology [15], and hydrology [16, 17], where it has often exhibited methodological and practical advantages over traditional kriging techniques. Its strengths become particularly evident in situations involving small sample sizes, highly heterogeneous spatial patterns, or considerable ambiguity in variogram parameter estimation. By integrating prior knowledge with observed information and accounting for the full posterior variability of model parameters, Bayesian Kriging generates prediction intervals that are statistically more defensible and reduces the risk of overly optimistic variance estimates commonly associated with ordinary kriging. Collectively, this probabilistic paradigm enhances model robustness and supports a more principled and transparent quantification of predictive uncertainty in spatial analysis [18].

Numerous prior studies have conducted comparative analyses between Bayesian Kriging and classical kriging methods or other interpolation methods, while others have concentrated exclusively on the implementation of Bayesian Kriging within specific empirical settings. These works typically evaluate predictive performance, uncertainty quantification, or methodological advantages under particular data conditions. Nevertheless, despite the expanding body of literature, systematic investigations into the performance of Bayesian Kriging across varying degrees of spatial autocorrelation remain scarce. In particular, studies that explicitly manipulate covariance parameters to generate different levels of spatial dependence and subsequently assess their impact on predictive accuracy are still limited. This shortcoming reveals a clear research gap, especially concerning the robustness of Bayesian Kriging under changing spatial autocorrelation structures. A rigorous understanding of the model's sensitivity to varying spatial conditions is essential to ensure its reliability and practical applicability across diverse real-world contexts, particularly rainfall data.

In rainfall data, the strength of spatial autocorrelation can differ between phases of the rainy season [19]. These differences provide an important setting for evaluating the robustness of Bayesian Kriging under changing spatial conditions. Regardless of whether spatial dependence is strong or weak, spatial interpolation remains essential in all seasonal phases. Accurate spatial prediction is crucial for hydrological analysis, disaster risk management,

agriculture, and water resource planning, making it important to use methods that perform reliably under varying rainfall patterns.

This study aims to evaluate the performance of Bayesian Kriging at various levels of spatial autocorrelation through a controlled simulation framework. The study was conducted by generating synthetic rainfall data at fixed observation points with systematically arranged variations in spatial autocorrelation levels. Furthermore, the prediction performance of the model was evaluated using error indicators such as Root Mean Square Error (RMSE) and Mean Absolute Error (MAE). Sensitivity analysis was performed separately on the early and peak phases of the rainy season to identify how changes in spatial dependency structures affect model accuracy and stability. Through this approach, the study is expected to provide a more comprehensive understanding of the robustness of Bayesian Kriging in dealing with varying spatial structures, particularly in daily rainfall interpolation.

2. Basic algorithm and extensions

2.1. Spatial Interpolation using Kriging

Spatial interpolation is a statistical technique used to estimate the value of a variable at unobserved locations based on information from available observation points. One of the most widely used geostatistical interpolation methods is Kriging, which explicitly incorporates spatial autocorrelation into the estimation process. The Kriging method was first developed by the South African mining engineer Danie G. Krige in the 1950s to estimate gold concentrations in the Witwatersrand mines. Theoretically, Kriging was developed as a Best Linear Unbiased Estimator (BLUE)[4]. This estimator constructs predictions as a weighted linear combination of observed values surrounding the location to be predicted. The weights are not determined solely by distance, but also by the spatial covariance structure derived from the variogram model. Let $Z(s)$ denote a stochastic process at location s. The Kriging estimator at an unobserved location s_0 is expressed as a linear combination of n observed values:

$$Z(s_0) = \Sigma \lambda_i \ Z(s_i), \ \ i = 1, \ldots, n \tag{1}$$

where λ_i represents the Kriging weights assigned to each observation $Z(s_i)$, and $Z(S_0)$ is the predicted value at location s_0 which satisfies the constraint $\Sigma\lambda_i = 1$. These weights are determined by minimizing the prediction variance subject to the unbiasedness constraint, ensuring that the estimator achieves minimum variance among all linear unbiased estimators.

An essential component in Kriging is the semivariogram, which characterizes the spatial variability structure of a variable [20]. The semivariogram describes the relationship between semivariance and the distance separating pairs of observation points. The three main parameters of a semivariogram model are the nugget, sill, and range. The nugget represents variability at very small distances or measurement error; the sill corresponds to the total variance when the separation distance becomes sufficiently large; and the range is the distance at which spatial correlation effectively disappears [21, 22]. Theoretical models such as spherical, exponential, and Gaussian are commonly used to fit the empirical semivariogram. The selection and estimation of variogram model parameters play a crucial role in determining interpolation accuracy, as the Kriging weights are derived from this variance structure. The spherical semivariogram model is one of the most commonly used theoretical models in geostatistics. It is defined as follows:

$$\gamma(h) = \begin{cases} \tau^2 + \sigma^2 \left(\dfrac{3h}{2\phi} - \dfrac{h^3}{2\phi^3} \right), & 0 < h \leq \phi \\ \tau^2 + \sigma^2, & h > \phi \end{cases} \tag{2}$$

In this model, $\gamma(h)$ denotes the semivariance at separation distance h. The parameter τ^2 represents the nugget effect, which accounts for microscale variability or measurement error. The parameter σ^2 corresponds to the partial sill, reflecting the structured spatial variance. The sum σ^2 is known as the partial sill, which represents the total variance once spatial correlation is no longer present. The parameter ϕ is the range, defined as the distance at which spatial correlation effectively disappears. The variable h indicates the separation distance between two spatial locations.

2.2. Bayesian Kriging

Bayesian Kriging in this study is formulated within a three-level hierarchical model that separates the observation process, the latent spatial process, and the model parameters [17]. The specification below corresponds to an Ordinary Kriging framework, where the mean is assumed constant but unknown.

Level 1: Data Model

$$Y(s_i) = Z(s_i) + \varepsilon(s_i), \qquad \varepsilon(s_i) \sim \mathcal{N}(0, \tau^2), \tag{3}$$

where $Y(s_i)$ denotes the observed value at location s_i, $Z(s_i)$ is the latent spatial process, and τ^2 represents the nugget variance accounting for measurement error and microscale variation.

Level 2: Process Model

$$Z(s) = \mu(s) + \delta(s), \tag{4}$$

$$\mu(s) = \beta_0, \tag{5}$$

$$\delta(s) \sim \mathcal{GP}\big(0, C(s, s'; \theta)\big), \tag{6}$$

where $\mu(s)$ is the mean function and is assumed to be constant over space, corresponding to the Ordinary Kriging assumption. The spatial dependence is captured by the zero-mean Gaussian process $\delta(s)$ with covariance function $C(s, s'; \theta)$, where $\theta = (\sigma^2, \phi)$, with σ^2 denoting the partial sill and ϕ the spatial range parameter.

Level 3: Parameter Model

$$\beta_0 \sim p(\beta_0) \propto 1, \qquad \sigma^2 \sim p(\sigma^2), \qquad \phi \sim p(\phi), \qquad \tau^2 \sim p(\tau^2). \tag{7}$$

A non-informative (flat) prior is assigned to β_0, which is consistent with the Bayesian formulation of Ordinary Kriging. The covariance parameters (σ^2, ϕ, τ^2) are assigned prior distributions and inferred from the data.

Thus, the posterior distribution is obtained as:

$$p(Z, \beta_0, \sigma^2, \phi, \tau^2 \mid Y) \propto p(Y \mid Z, \tau^2)\, p(Z \mid \beta_0, \sigma^2, \phi)\, p(\beta_0)\, p(\sigma^2)\, p(\phi)\, p(\tau^2). \tag{8}$$

In the simulation study, each generated dataset is treated as an independent realization of the spatial process. For every simulated dataset, the model parameters $(\beta_0, \sigma^2, \phi, \tau^2)$ are re-estimated using the Bayesian kriging procedure implemented via the grid-based approximation approach. This ensures that the simulation evaluates the full parameter estimation process rather than assuming known parameters.
Through this formulation, Bayesian Kriging not only produces point predictions $\widehat{Z}(s_0)$, but also the full posterior predictive distribution:

$$p\big(Z(s_0) \mid Y\big). \tag{9}$$

This formulation explicitly represents parameter uncertainty and spatial structure simultaneously. The predictive posterior at a new location s_0 is obtained by integrating uncertainty over the latent process and model parameters. In general, it can be written as:

$$p\big(Z(s_0) \mid Y\big) = \int\int p\big(Z(s_0) \mid Z, \theta, Y\big)\, p(Z, \theta \mid Y)\, dZ\, d\theta. \tag{10}$$

The equation shows that the predictive posterior is the weighted average of the conditional predictive distribution, where the weights are given by the joint posterior distribution of the latent process and parameters. This is the fundamental difference from Ordinary Kriging, which relies on point estimates of the covariance parameters without integrating over parameter uncertainty. The posterior predictive distribution has two important components: the posterior mean, which serves as the point prediction, and the posterior variance, which quantifies prediction uncertainty.

2.3. Implementation of Grid-Based Approximation

Bayesian inference in this study was conducted using a grid-based discrete approximation approach, following the framework introduced by Tanner and Wong. This approach approximates the posterior distribution of covariance parameters by discretizing part of the parameter space and combining it with conditional sampling to obtain posterior realizations [23, 24]. In this approach, the covariance parameter space, for example $\theta = (\beta, \sigma^2, \phi, \tau^2)$, is discretized into a set of predetermined grid points. For each parameter combination on the grid, the likelihood function $p(Y \mid \theta)$ is computed under the assumption of a spatial Gaussian process, and then multiplied by the prior distribution $p(\theta)$ to obtain the unnormalized posterior weight. The posterior distribution of the parameters is then obtained by normalizing all weights across the grid, so that the continuous integral in the Bayesian formulation is approximated by a discrete summation over the grid.

The implementation was performed using the `krige.bayes()` function from the `geoR` package in R [24]. In accordance with this implementation, the discretization is applied primarily to the range parameter (ϕ), while the remaining parameters are handled through conditional posterior distributions. Specifically, ϕ is defined over a finite support and assigned a discrete uniform prior. In this study, the support of ϕ is determined internally by the function based on the spatial configuration of the data, particularly the distribution of inter-site distances. Although the grid is not explicitly specified in the code, the function automatically constructs a fixed (non-adaptive) grid of candidate values for ϕ within a plausible interval related to the maximum distance among observation locations.

For the partial sill (σ^2), a reciprocal prior is specified (`sigmasq.prior = "reciprocal"`), and inference is performed through conditional sampling given ϕ. The nugget effect (τ^2) is also treated as an unknown parameter and estimated within the covariance structure, with its initial value informed by a proportion of the sample variance, as defined in the preliminary likelihood-based estimation (likfit). The mean parameter (β) is assigned a flat prior (`beta.prior = "flat"`), reflecting a non-informative assumption. Therefore, explicit grid discretization is only applied to ϕ, while β and σ^2 are sampled conditionally from their respective posterior distributions.

The computational procedure follows a hybrid scheme. First, the posterior distribution of ϕ is approximated on the discrete grid constructed internally. Then, values of ϕ are sampled according to their posterior probabilities. Conditional on each sampled ϕ, the parameters β and σ^2 are subsequently drawn from their conditional posterior distributions. This process is repeated to obtain samples from the joint posterior distribution, which are then used to compute predictive summaries at unobserved locations. The range of ϕ and the associated grid are implicitly determined from the data, particularly through the spatial extent and variability reflected in the empirical variogram and inter-point distances. While the exact number of grid points is not manually specified, the default setting in the function ensures a sufficient resolution for stable posterior approximation.

2.4. Study Area and Data Source

The study area of this research is East Java, located in the eastern part of Java Island, Indonesia. The province is characterized by a tropical monsoon climate with pronounced seasonal variability in rainfall patterns. Its climatic conditions are strongly influenced by the Asian–Australian monsoon system, resulting in distinct wet and dry seasons each year. The data used in this study were obtained from the *Badan Meteorologi, Klimatologi, dan Geofisika* (BMKG), the official Indonesian governmental agency responsible for meteorological and climatological observations. The dataset consists of daily rainfall records from 2019 to 2024 collected from 38 observation stations distributed across East Java. The study area is shown in Figure 1.

Daily rainfall refers to the total amount of precipitation accumulated over a 24-hour period at a specific observation site, typically measured in millimeters (mm). Operationally, rainfall data are recorded using standardized rain gauges that measure the depth of precipitation within a fixed daily observation interval. Daily rainfall data commonly contain missing values in secondary meteorological datasets due to recording errors or instrument limitations. In this study, missing values were addressed during the aggregation process by calculating the average daily rainfall for each station using only the available observations. Specifically, the onset phase and peak phase were defined, and the mean rainfall for each phase was computed by excluding missing entries. Daily rainfall data are widely used in hydrological analysis, water resource management, flood risk assessment, climate variability studies, and spatial modeling applications [25]. Compared to monthly or annual aggregates, daily data

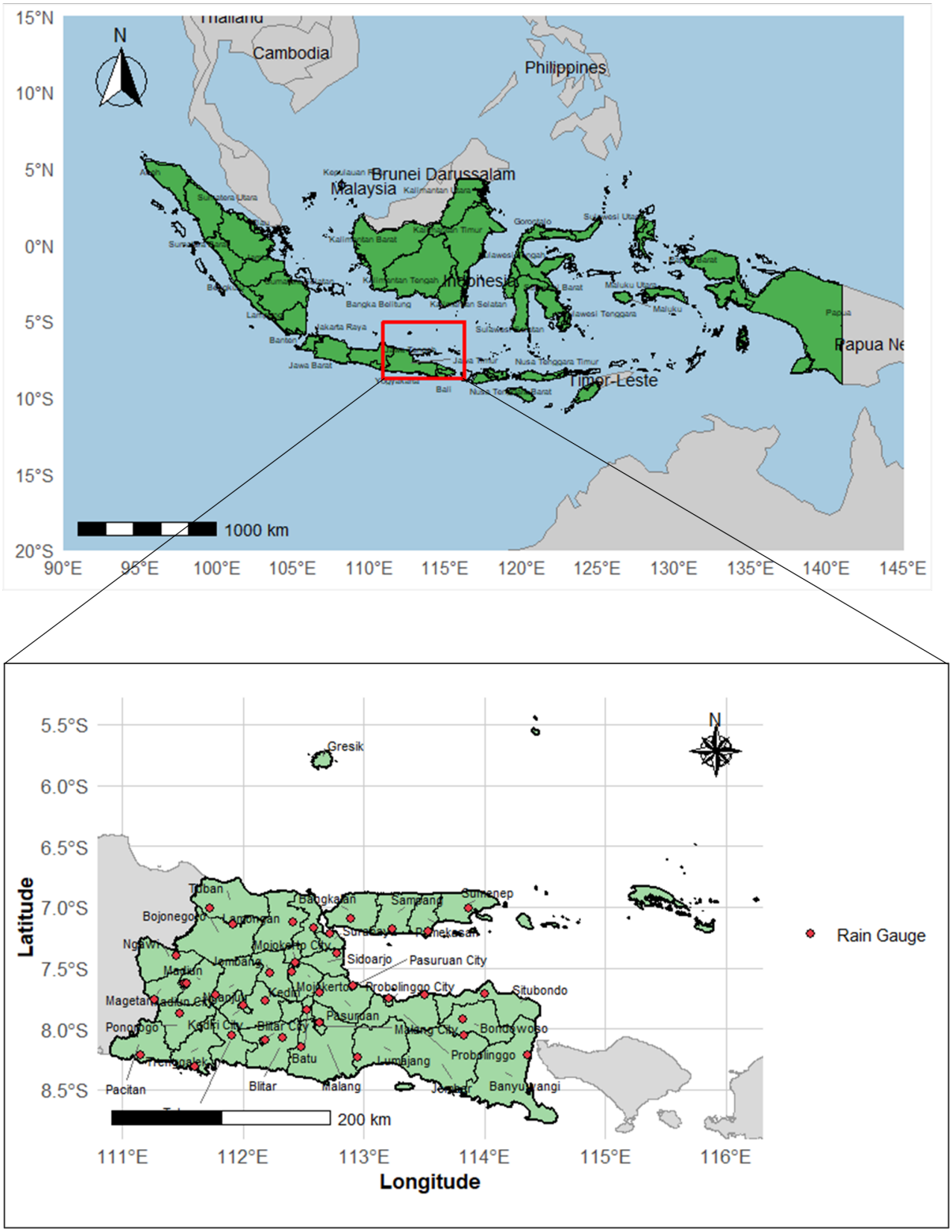

Figure 1. Study Area in East Java Province, Indonesia, and Locations of Rain Gauge Used in This Study

provide higher temporal resolution, enabling a more detailed assessment of rainfall intensity, variability, and spatial dependence.

To capture seasonal differences in spatial rainfall characteristics, the data were divided into two phases of the rainy season: the onset phase (September–November) and the peak phase (December–February) [26]. The onset phase marks the transition period when rainfall frequency and intensity begin to increase due to the shift in monsoonal circulation. During this phase, rainfall systems are often regionally organized, potentially resulting in strong spatial autocorrelation. The peak rainy season represents the period of highest rainfall intensity within the annual cycle, characterized by intensified convective activity and large-scale atmospheric dynamics. However, this phase may exhibit lower spatial autocorrelation due to the dominance of widespread yet localized convective processes. Rainfall during this period tends to develop rapidly and independently across locations, resulting in high variability over short distances. In contrast to the onset phase, which is influenced by more organized large-scale systems that produce coherent spatial patterns, rainfall in the peak phase is more randomly distributed. Consequently, spatial continuity weakens, leading to lower or negligible spatial autocorrelation.

This seasonal classification allows for a comparative analysis of spatial variability structures and autocorrelation patterns, which are essential for evaluating the performance of the spatial interpolation methods applied in this study.

2.5. Simulation Study

A simulation study was conducted to evaluate the performance and robustness of Bayesian Kriging for daily rainfall interpolation in East Java. The empirical data consist of daily rainfall observations analyzed separately for the onset and peak phase of the rainy season. The primary objective is to assess how the predictive performance of Bayesian Kriging behaves under varying levels of spatial autocorrelation.

Synthetic rainfall datasets were generated while preserving the spatial coordinates of the 38 observation points. The simulation design is grounded on the semivariogram parameters previously estimated from the Bayesian Kriging interpolation of the real data. Specifically, the sill and nugget parameters were fixed according to the estimated values from each phase, ensuring that the variance structure remains consistent with empirical characteristics.

The range parameter was sistematically varied as a proxy for spatial autocorrelation strength. A Range Factor was introduced and defined as the ratio between the simulated range parameter and the baseline (estimated) range parameter

$$\text{Range Factor} = \frac{\phi_{simulated}}{\phi_{estimated}}$$

In this study, ten Range Factor values (0.3 to 3) were used to represent a gradient from weak to strong spatial dependence. For each scenario, rainfall fields were generated using a stationary and isotropic Gaussian random field based on the specified semivariogram model. Each scenario was repeated 50 times to ensure stale performance estimates. The simulation framework consisted the following steps:

1. Estimation of baseline semivariogram parameters.
2. Adjustment of the range using Range Factor.
3. Simulation of rainfall data.
4. Application of Bayesian Kriging.
5. Evaluation using RMSE and MAE
6. Quantification of spatial autocorrelation using Moran's I.

By recording Moran's I values across simulations, the study provides an empirical link between the theoretical semivariogram specification and the observed spatial dependence structure. Model performance was evaluated using RMSE and MAE, which are widely used in geoscientific modeling. RMSE is sensitive to large errors and is commonly applied in meteorology and climate studies, while MAE provides a robust measure of average error. As no single metric is universally superior, their combined use offers a more comprehensive assessment of predictive performance [27, 28].

3. Experimental results

3.1. Exploratory Spatial Data Analysis

Exploratory Spatial Data Analysis (ESDA) was conducted to obtain a comprehensive preliminary understanding of the statistical and spatial characteristics of daily rainfall data in East Java during two seasonal phases: the onset phase and the peak phase of the rainy season. This analysis aims to identify distributional patterns, variability levels, and the presence of spatial autocorrelation prior to implementing Bayesian Kriging interpolation. The descriptive statistics reveal clear differences in rainfall characteristics between the onset phase and the peak phase of the rainy season in East Java. The descriptive statistics reveal clear differences in rainfall characteristics between the onset phase and the peak phase of the rainy season in East Java is shown in Table 1.

Table 1. Descriptive Statistics of Daily Rainfall by Seasonal Phase

Phase	Mean	Standard Deviation	Minimum	Maximum	CV
Onset	4.338280	2.268149	1.313112	11.94283	0.5228222
Peak	9.959336	2.251065	5.114572	16.52302	0.2260257

During the onset phase, the mean daily rainfall is 4.34 mm, with a standard deviation of 2.27 mm. The minimum and maximum values range from 1.31 mm to 11.94 mm, indicating a relatively wide spread of rainfall intensities across observation stations. The Coefficient of Variation (CV) is 0.52, suggesting substantial relative variability. A CV greater than 0.5 indicates that rainfall distribution during the onset phase is moderately heterogeneous across space. This implies that certain areas experience noticeably higher rainfall than others, which may contribute to stronger localized spatial contrasts.

During the peak phase, the mean daily rainfall increases significantly to 9.96 mm, more than double that of the onset phase. However, despite the higher average rainfall, the standard deviation (2.25 mm) is similar in magnitude to that of the onset phase. As a result, the coefficient of variation decreases to 0.23, indicating substantially lower relative variability. This suggests that rainfall during the peak phase is more spatially homogeneous, with values that are more evenly distributed across the 38 observation locations.

Based on the spatial distribution of rainfall in East Java presented in Figure 2, the daily rainfall patterns exhibit distinct characteristics between the two seasonal phases. During the onset phase of the rainy season (Figure 2a), daily rainfall demonstrates greater spatial variability across locations. Rainfall intensity is relatively uneven, with certain areas recording substantially higher values compared to neighboring regions. This pattern suggests that the onset period is still influenced by atmospheric transition processes, resulting in a spatial distribution that has not yet reached homogeneity. Local variability remains pronounced, particularly in areas affected by topographic factors such as mountainous regions and the southern part of East Java. During the peak phase of the rainy season (Figure 2b), the spatial distribution of daily rainfall appears more uniform across the region. Rainfall intensity is generally high at most stations, and the differences between locations are less pronounced compared to the onset phase. This indicates that during the peak season, the atmospheric system becomes more established and dominant, leading to more widespread and synchronous rainfall across East Java.

3.2. Spatial Autocorrelation

From the spatial distribution map of the observation points in Figure 1, the onset phase of the rainy season exhibits visible clustering of similar rainfall values in several areas. This pattern indicates the presence of relatively strong spatial autocorrelation, where geographically proximate locations tend to record comparable levels of daily rainfall. The pronounced spatial variability during this phase often gives rise to a clearly defined spatial dependence structure. During the peak phase of the rainy season, although rainfall occurs more extensively across the region, the differences in magnitude between locations become less distinct. This reduced contrast may lead to relatively weaker spatial autocorrelation compared to the onset phase, as the spatial variability is more homogeneous. Statistically, the degree of spatial dependence among rainfall observations can be formally assessed using Moran's

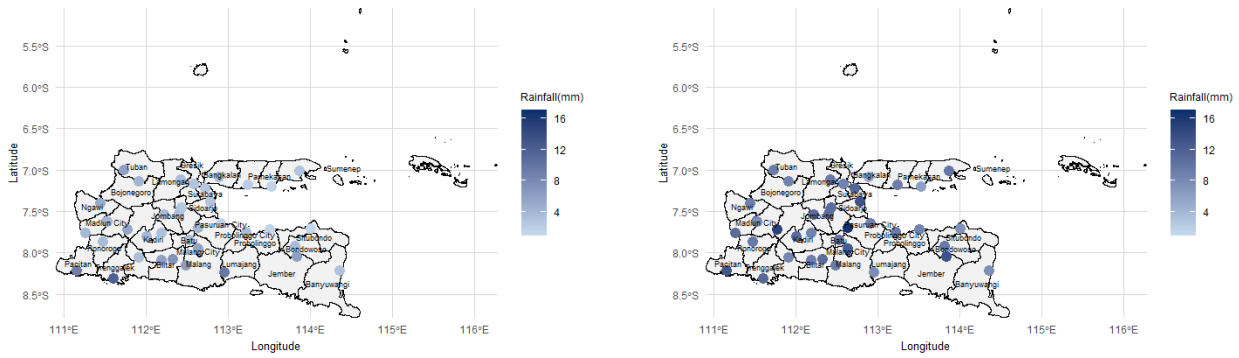

(a) Onset Phase (b) Peak Phase

Figure 2. Spatial Distribution of Daily Rainfall during Onset and Peak Phases

I test, as presented in Table 2. In general, Moran's I values close to zero indicate weak or random spatial patterns, values between approximately 0.2–0.3 indicate moderate spatial dependence, and values greater than 0.3 suggest strong spatial dependence.

Table 2. Global Moran's I Results for Daily Rainfall by Seasonal Phase

Phase	Moran's I Statistic	P-value	Explanation
Onset	0.2337	0.0011	Significant moderate positive spatial autocorrelation
Peak	0.0094	0.3368	No significant spatial autocorrelation (spatially random pattern)

The results of the Global Moran's I indicate contrasting spatial dependence patterns between the two seasonal phases. During the onset phase of the rainy season, the Global Moran's I reveals significant positive spatial autocorrelation, suggesting that daily rainfall values tend to form geographic clusters. This means that nearby locations are more likely to exhibit similar rainfall intensities, reflecting a clearly structured spatial pattern. During the peak phase of the rainy season, the Global Moran's I does not indicate significant spatial autocorrelation. This implies that the spatial distribution of daily rainfall is relatively random, with no strong evidence of systematic clustering across locations.

3.3. Variogram Parameter Estimation using Bayesian

The spatial dependence of daily rainfall during the onset phase was modeled within a Bayesian geostatistical framework employing a spherical covariance structure. Under this specification, the key parameters of the variogram were inferred from their posterior distributions rather than estimated solely through classical likelihood maximization. This Bayesian formulation enables explicit propagation of parameter uncertainty into the kriging predictions, thereby yielding a more probabilistically coherent representation of spatial variability. The empirical variogram is shown in Figure 3.

The empirical variogram for the onset phase reveals a systematic increase in semivariance with distance, followed by stabilization around the sill, indicating a well-defined and spatially structured dependence pattern. Low semivariance at short separation distances reflects strong local similarity in rainfall intensity, while the gradual rise toward the sill signifies progressive decorrelation as inter-site distance increases. The fitted spherical model closely approximates the empirical pattern, particularly along the ascending limb of the variogram, suggesting that the assumed covariance structure adequately characterizes the underlying spatial process. The relatively gradual

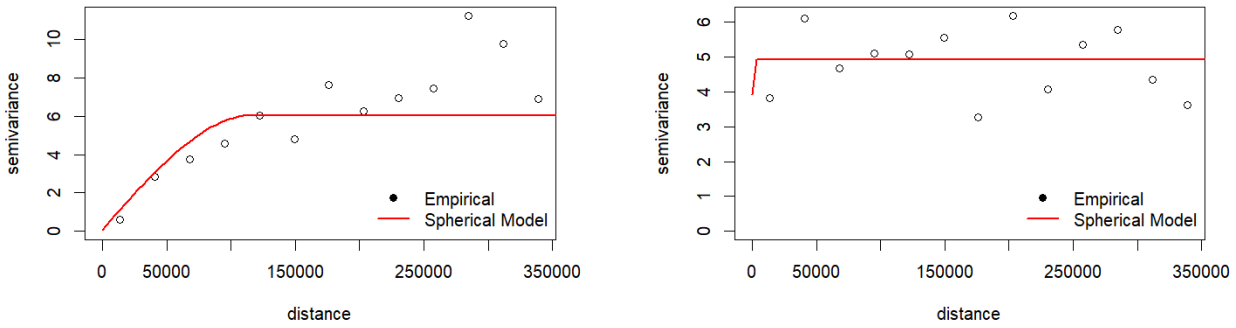

(a) Onset Variogram

(b) Peak Variogram

Figure 3. Empirical variograms and fitted spherical models for (a) onset and (b) peak phases of the rainy season. The x-axis denotes the separation distance between observation points (in meters), and the y-axis denotes semivariance (in mm²), representing the variability of rainfall as a function of distance.

attainment of the sill further implies that spatial autocorrelation persists over a substantial spatial extent, consistent with organized mesoscale atmospheric dynamics that typify the transitional onset period.

The variogram corresponding to the peak phase exhibits a comparatively attenuated structure. The semivariance displays a weaker and less systematic relationship with distance, and the spherical model approaches the sill more rapidly, indicating a shorter effective correlation range. This pattern suggests that spatial dependence decays more abruptly, implying reduced spatial contrast among neighboring locations. The broader dispersion of empirical variogram points also reflects a more homogeneous rainfall regime, wherein precipitation occurs more uniformly across the study region.

These results demonstrate that spatial dependence is more pronounced and spatially extensive during the onset phase, whereas the peak phase is characterized by a more spatially homogeneous rainfall distribution with diminished correlation strength. This contrast underscores the seasonal modulation of rainfall-generating mechanisms, with transitional conditions fostering stronger spatial structuring and peak-season dynamics promoting broader spatial uniformity.

From the Bayesian parameter estimates, which are shown in 2, the onset phase exhibits a relatively small nugget effect compared to the structured variance (sill), indicating that most of the rainfall variability is explained by spatially correlated processes rather than micro-scale noise. The estimated spatial range is substantial, implying that spatial correlation extends over a considerable distance, consistent with the gradual increase of the empirical variogram and the persistence of spatial continuity. In contrast, the peak phase demonstrates a markedly different structure: the nugget variance dominates, while the structured spatial variance is negligible and the effective range collapses toward zero. This configuration indicates that rainfall variability during the peak season is primarily unstructured, with minimal spatial continuity captured by the covariance model.

During the peak phase, both the estimated sill ($\hat{\sigma^2}$) and spatial range ($\hat{\phi}$) are equal to zero. In a spherical covariance framework, this result implies that the spatially structured component of variability vanishes entirely. When $\hat{\sigma}^2 = 0$, there is no structured spatial variance, and when $\hat{\phi} = 0$, spatial correlation does not extend beyond infinitesimal distance. Consequently, the covariance model reduces to a pure nugget process, meaning that rainfall variability is dominated entirely by unstructured, local-scale variation ($\hat{\tau}^2$). In practical terms, this indicates that daily rainfall during the peak season does not exhibit measurable spatial dependence at the scale of observation. Rainfall amounts at neighboring stations behave as if they are statistically independent. Such a condition is consistent with rainfall generated by localized convective systems that produce intense but spatially irregular precipitation, thereby weakening regional-scale spatial continuity.

Table 3. Parameter Estimates and Prediction Accuracy by Seasonal Phase

Parameter Estimation	Onset Phase	Peak Phase
$\hat{\beta}$	4.3382	9.9593
$\hat{\sigma}^2$	5.9817	0.0000
$\hat{\phi}$	117530.1	0.0000
$\hat{\tau}^2$	0.0712	4.9339
RMSE	1.6418	2.3121
MAE	1.2167	1.7638

The onset phase shows a positive sill ($\hat{\sigma}^2$) and a substantial spatial range ($\hat{\phi} \approx 117,530$). This indicates the presence of meaningful spatial structure, where rainfall values remain correlated over a considerable distance. The relatively small nugget effect ($\hat{\tau}^2$) further suggests that most variability is explained by structured spatial processes rather than random noise. This pattern is typical of transitional seasonal dynamics, where mesoscale atmospheric mechanisms generate organized and spatially coherent rainfall fields.

The predictive performance, as measured by RMSE and MAE, indicates that the Bayesian kriging model performs better during the onset phase than during the peak phase. The lower RMSE and MAE values in the onset period imply smaller average and extreme deviations between observed and predicted daily rainfall, reflecting higher interpolation accuracy. In practical terms, this means that rainfall estimates during the onset phase are more reliable, likely due to the presence of meaningful spatial dependence that enhances the effectiveness of spatial prediction. The higher RMSE and MAE values in the peak phase indicate larger prediction errors, both on average and in extreme cases. This reduced accuracy is consistent with the absence of spatial structure during the peak season, where rainfall variability is dominated by local randomness, limiting the ability of neighboring observations to improve prediction.

These findings highlight that the strength and extent of spatial autocorrelation—particularly the magnitude of the spatial range—directly influence the performance of Bayesian kriging. However, empirical data alone do not allow full control over the spatial range parameter, making it difficult to systematically evaluate how varying levels of spatial dependence affect predictive accuracy. Therefore, a simulation study becomes essential. By generating spatial data under controlled range settings, the simulation framework enables a structured investigation of how different degrees of spatial continuity influence parameter estimation stability and prediction performance. This approach provides a deeper understanding of the sensitivity of Bayesian kriging to the spatial range parameter and justifies the need for a controlled simulation experiment in the subsequent section.

3.4. The Results of the Simulation Study

The simulation study was conducted to evaluate the sensitivity of Bayesian kriging performance to different levels of spatial dependence, particularly with respect to the spatial range parameter. The initial empirical estimation for the peak phase indicated that the partial sill ($\hat{\sigma}^2$) was effectively zero, suggesting the absence of spatially structured variation (a pure nugget effect). Under such conditions, variation in the range parameter ($\hat{\phi}$) becomes theoretically irrelevant, as the covariance function does not depend on distance. In response to this issue, a substantial revision to the simulation design was implemented. Specifically, the value of $\hat{\sigma}^2$ for the peak phase scenario was no longer fixed at the empirically estimated value of zero. Instead, a positive (nonzero) $\hat{\sigma}^2$ was adopted, with magnitude comparable to the variability observed in the onset phase, in order to ensure the presence of a meaningful spatial structure. With this adjustment, variation in the range parameter ($\hat{\phi}$) becomes relevant and allows for a valid evaluation of the sensitivity of Bayesian kriging performance to different levels of spatial autocorrelation. The summary of the simulation study is shown in Table 4.

The simulation results demonstrate a clear contrast in how spatial range influences Bayesian kriging performance between the onset and peak phases. In the onset scenario, increasing the range factor systematically increases Moran's I, indicating strengthening spatial autocorrelation, which is followed by a consistent reduction in RMSE

Table 4. Sensitivity Analysis of Range Factor under Different Seasonal Phases

Phase	Scenario	Range Factor	Range Used (m)	Moran's I	RMSE	MAE
Onset	1	0.3	35259.03	0.0053	2.3105	1.8190
	2	0.6	70518.06	0.2083	1.8739	1.4750
	3	0.9	105777.1	0.3101	1.6107	1.2663
	4	1.2	141036.1	0.4489	1.3654	1.0630
	5	1.5	176295.2	0.4974	1.2312	0.9686
	6	1.8	211554.2	0.4337	1.1418	0.8982
	7	2.1	246813.2	0.5132	1.0953	0.8478
	8	2.4	282072.2	0.5417	0.9576	0.7477
	9	2.7	317331.3	0.4652	0.9621	0.7540
	10	3.0	352590.3	0.5447	0.9368	0.7284
Peak	1	0.3	35259.03	-0.0024	3.1320	2.4988
	2	0.6	70518.06	0.1162	2.9692	2.4059
	3	0.9	105777.1	0.1808	2.9798	2.3921
	4	1.2	141036.1	0.1959	2.7690	2.2183
	5	1.5	176295.2	0.1835	2.7021	2.1560
	6	1.8	211554.2	0.1638	2.6920	2.1608
	7	2.1	246813.2	0.1943	2.6445	2.1283
	8	2.4	282072.2	0.1840	2.5594	2.0571
	9	2.7	317331.3	0.1574	2.5190	2.0311
	10	3.0	352590.3	0.1371	2.6105	2.0995

and MAE. Figure 4 confirms that stronger and more extensive spatial dependence substantially improves predictive accuracy, as neighboring observations provide increasingly informative contributions to kriging estimates. The decline in RMSE from above 2.3 to below 1.0 as the range expands illustrates the sensitivity of Bayesian kriging to the spatial continuity parameter.

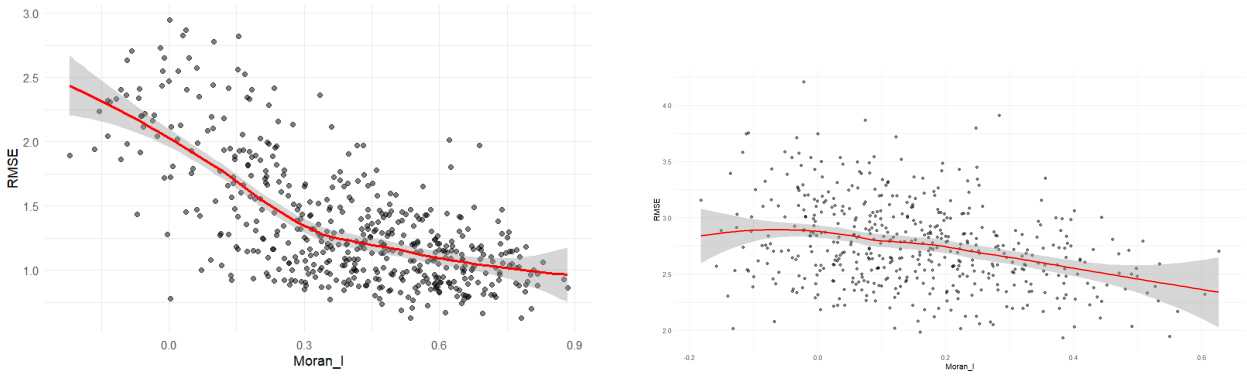

(a) Onset (b) Peak

Figure 4. Scatter plot of Moran's I versus RMSE under different spatial range settings

The peak phase in Figure 4 shows persistently weak Moran's I values across all range scenarios and only marginal reductions in RMSE and MAE. Even when the imposed range increases, prediction errors remain relatively high and decrease only slightly, indicating that artificially enlarging the range cannot compensate for inherently weak spatial structure. The accompanying visualization further reinforces this relationship: the scatterplot shows a clear negative association between Moran's I and RMSE, with the smoothed trend line declining as spatial

autocorrelation strengthens. This graphical pattern empirically confirms that higher spatial autocorrelation leads to lower prediction error, thereby validating the theoretical expectation that the effectiveness of Bayesian kriging is strongly governed by the magnitude and extent of spatial dependence.

Bayesian kriging is theoretically grounded in the assumption that spatial dependence exists and can be modeled through a structured covariance function. When spatial autocorrelation is absent or weak, the spatial signal becomes indistinguishable from random noise, and the kriging predictor increasingly resembles a global mean estimator with a dominant nugget effect. Under such conditions, although Bayesian kriging remains statistically coherent, because parameter uncertainty is formally incorporated through prior distributions, the predictive advantage of spatial borrowing diminishes substantially. In other words, the model is valid but no longer efficient in extracting meaningful spatial structure for interpolation.

Based on the simulation results, the performance of Bayesian kriging is strongly associated with the magnitude of spatial autocorrelation as measured by Moran's I. When Moran's I is close to zero (approximately < 0.2), the reduction in RMSE is minimal, and predictive performance remains relatively poor. This pattern is clearly observed in the peak phase simulation, where Moran's I values are predominantly below 0.2, the RMSE remains high and only slightly decreases despite increasing spatial range. This indicates that under weak spatial dependence (Moran's $I < 0.20$), Bayesian kriging cannot effectively exploit neighboring information, resulting in limited interpolation improvement.

The onset phase simulation demonstrates a marked improvement in predictive accuracy once spatial autocorrelation reaches moderate levels. A substantial decline in RMSE becomes evident when Moran's I exceeds approximately 0.20, with performance improving more sharply beyond $0.20-0.30$. When Moran's I approaches 0.30 or higher, the model achieves its lowest RMSE values, indicating that strong positive spatial autocorrelation provides sufficient structural information for highly accurate interpolation. Thus, empirically, the simulation suggests that Bayesian kriging performs very well when Moran's $I \geq 0.30$, and becomes clearly optimal when Moran's $I \geq 0.40$. Conversely, its performance deteriorates markedly when Moran's I falls below approximately 0.20.

These findings reinforce a fundamental principle of geostatistics: the effectiveness of Bayesian Kriging is contingent upon the presence of meaningful spatial dependence. Moderate to strong spatial autocorrelation enables reliable spatial smoothing and borrowing of strength across neighboring locations, while weak or absent autocorrelation reduces the interpolation process to near-random prediction with limited spatial gain.

4. Conclusion

This study demonstrates that the effectiveness of Bayesian kriging in spatial interpolation is fundamentally determined by the strength of spatial autocorrelation. Although Bayesian kriging remains statistically valid under all spatial conditions due to its probabilistic framework and incorporation of parameter uncertainty, its predictive performance is highly sensitive to the magnitude of spatial dependence. When spatial autocorrelation is weak, the model yields only marginal improvements in prediction accuracy, as spatial information contributes limited explanatory power. In such cases, the interpolation process is largely dominated by the nugget effect, and the benefits of spatial modeling are substantially reduced.

The simulation results indicate that Bayesian kriging performs substantially better once spatial autocorrelation reaches moderate levels. A meaningful improvement in interpolation accuracy becomes evident when Moran's I exceeds approximately 0.20, with performance becoming clearly optimal when Moran's I is greater than 0.30. Under strong spatial autocorrelation (Moran's $I \geq 0.40$), the model achieves its lowest prediction errors, confirming that structured spatial dependence provides the necessary information for reliable spatial smoothing and accurate estimation. These findings highlight that Bayesian kriging is not fully robust in environments characterized by weak spatial autocorrelation. Its practical advantage emerges primarily in settings where moderate to strong spatial dependence exists. Therefore, assessing the magnitude and significance of spatial autocorrelation should be considered a critical preliminary step before applying Bayesian kriging for spatial interpolation.

This study has several limitations that should be acknowledged. First, the conclusions are derived from controlled simulation scenarios in which spatial range and autocorrelation strength were systematically manipulated. Although simulations allow clear isolation of spatial effects, real-world spatial processes are often more complex, involving anisotropy, non-stationarity, irregular sampling, and measurement error that were not fully represented in the experimental design. In the simulation design, the spatial variance and baseline range parameters used for the peak phase were adopted from the onset phase estimation to ensure a consistent spatial structure across scenarios. While this approach improves comparability, it may not fully capture the intrinsic spatial characteristics of the peak phase. Second, spatial dependence was primarily evaluated using Moran's I as a global indicator. While Moran's I provides a useful summary of spatial autocorrelation, it may not fully capture local clustering patterns or multiscale spatial structures that can also influence kriging performance.

An initial assessment of spatial autocorrelation should be undertaken prior to implementing Bayesian kriging, as the magnitude and statistical salience of spatial dependence directly govern its predictive utility. When Moran's I falls below approximately $0.15-0.20$ and lacks statistical significance, the anticipated gains from spatial interpolation are typically attenuated, implying that alternative modeling strategies—such as non-spatial regression frameworks or hierarchical specifications incorporating pertinent covariates—may yield comparable or even more parsimonious performance. Conversely, when Moran's I exceeds 0.30, signifying moderate to strong spatial dependence, Bayesian kriging may be deployed with heightened confidence, since the presence of a structured spatial signal markedly augments interpolation fidelity. To enhance the external validity and inferential breadth of these findings, subsequent investigations should broaden the simulation architecture to accommodate more intricate spatial phenomena, including non-stationary dynamics, anisotropic covariance configurations, heterogeneous sampling regimes, and alternative prior formulations.

Acknowledgement

We would like to express our gratitude to the Rector of Universitas Brawijaya and DRPM for providing financial support in the Penelitian Dasar Madya grant, 2025. We are also thankful to the anonymous reviewers for the valuable comments and suggestions on the earlier draft paper.

REFERENCES

1. G. Uma, and B. R. Sneha, *A Study on the Footprints of Rainfall Pattern for a Sustainable Climate*, International Journal For Multidisciplinary Research, vol. 5, no. 4, p. 4400, 2023.
2. M. A. Amini, G. Torkan, S. Eslamian, M. J. Zareian, and J. F. Adamowski, *Analysis of deterministic and geostatistical interpolation techniques for mapping meteorological variables at large watershed scales*, Acta Geophysica, vol. 67, no. 1, pp. 191–203, 2019.
3. P. Singh, and P. Verma, *A Comparative Study of Spatial Interpolation Technique (IDW and Kriging) for Determining Groundwater Quality*, GIS and Geostatistical Techniques for Groundwater Science, Elsevier, pp. 43–56, 2019.
4. D. E. Myers, *Interpolation and estimation with spatially located data*, Chemometrics and Intelligent Laboratory Systems, vol. 11, no. 3, pp. 209–228, 1991.
5. P. Biernacik, W. Kazimierski, and M. Włodarczyk-Sielicka, *Comparative Analysis of Selected Geostatistical Methods for Bottom Surface Modeling*, Sensors, vol. 23, no. 8, p. 3941, 2023.
6. M. Ohmer, T. Liesch, N. Goeppert, and N. Goldscheider, *On the optimal selection of interpolation methods for groundwater contouring*, Advances in Water Resources, vol. 109, pp. 121–132, 2017.
7. M. Wieskotten, M. Crozet, B. Iooss, C. Lacaux, and A. Marrel, *A Comparison Between Bayesian and Ordinary Kriging Based on Validation Criteria*, Mathematical Geosciences, vol. 56, no. 1, pp. 143–168, 2024.
8. J. Pilz, and G. Spöck, *Why do we need and how should we implement Bayesian kriging methods*, Stochastic Environmental Research and Risk Assessment, vol. 22, no. 5, pp. 621–632, 2008.
9. A. Gribov, and K. Krivoruchko, *Empirical Bayesian kriging implementation and usage*, Science of The Total Environment, vol. 722, p. 137290, 2020.
10. A. O. Lima, G. B. Lyra, M. C. Abreu, J. F. Oliveira-Júnior, M. Zeri, and G. Cunha-Zeri, *Extreme rainfall events over Rio de Janeiro State, Brazil*, Atmospheric Research, vol. 247, p. 105221, 2021.
11. A. Verdin, B. Rajagopalan, W. Kleiber, and C. Funk, *A Bayesian kriging approach for blending satellite and ground precipitation observations*, Water Resources Research, vol. 51, no. 2, pp. 908–921, 2015.
12. C. Singha, and K. C. Swain, *Assessing The Spatial Variability of Soil Nutrients Prediction Using GIS-based Interpolation Techniques*, IEEE World Conference on Applied Intelligence and Computing (AIC), pp. 757–763, 2022.

13. L. Wang. r. Liu, J. Liu, Y. Qi, W. Zeng, and B. Cui, *A novel regional-scale human health risk assessment model for soil heavy metal(loid) pollution based on empirical Bayesian kriging*, Ecotoxicology and Environmental Safety, vol. 258, p. 114953, 2023.
14. C. E. L. Gilder, M. M. Othman, C. Zapata, E. A. Holcombe, R. De Risi, F. De Luca, and P. J. Vardanega, *Use of Bayesian Kriging to develop new soil property maps for Quito, Ecuador*, Geotechnical Engineering Challenges to Meet Current and Emerging Needs of Society, CRC Press, pp. 1131–1135, 2024.
15. Md. F. Hossen, and N. Sultana, *Landscape transition-induced ecological risk modeling using GIS and remote sensing techniques*, Environmental Monitoring and Assessment, vol. 196, no. 10, p. 964, 2024.
16. S. Astutik et al., *Leveraging the Bayesian Model's Posterior Distributions to Enhance the Accuracy of Rainfall Predictions*, Advanced Mathematical Models & Applications, vol. 10, no. 3, pp. 553–567, 2025.
17. R. H. P. Y. Damayanti, S. Astutik, and A. B. Astuti, *An Informative Prior of Bayesian Kriging Approach for Monthly Rainfall Interpolation in East Java*, Jurnal Teori dan Aplikasi Matematika, vol. 9, no. 3, p. 752, 2025.
18. S. H. Ng, and J. Yin, *Bayesian Kriging Analysis and Design for Stochastic Simulations*, ACM Transactions on Modeling and Computer Simulation, vol. 22, no. 3, pp. 1–26, 2012.
19. J. Israelsson, E. Black, C. neves, F. F. Torgbor, H. Greatrex, M. Tau, and P. N. L. Lamptey, *The spatial correlation structure of rainfall at the local scale over southern Ghana*, Journal of Hydrology: Regional Studies, vol. 31, p. 100720, 2020.
20. M. A. Oliver, and R. Webster, *Basic steps in geostatistics: the variogram and kriging*, Cham, Switzerland: Springer International Publishing. 2015
21. R. A. Olea, *A six-step practical approach to semivariogram modeling*, Stochastic Environmental Research and Risk Assessment, vol. 20, no. 5, pp. 307–318, 2006.
22. N. T. Sugito, I. Gumilar, A. Hernandi, A. P. Handayani, and M. Dede. *Utilizing semi-variograms and geostatistical approach for land value model in urban region*, International Journal of Engineering, vol. 36, no. 12, pp. 2222–2231, 2023.
23. M. A. Tanner, *Tools for Statistical Inference: Methods for the Exploration of Posterior Distributions and Likelihood Functions*, New York: Springer, 1996.
24. P. J. Jr. Ribeiro and P. J. Diggle *Bayesian inference in Gaussian model-based geostatistics* Tech. Report ST-99-08, Dept Maths and Stats, Lancaster University. 1999.
25. S. K. Sharma, Y. J. Kwak, R. Kumar, and B. Sharma, *Analysis of hydrological sensitivity for flood risk assessment*, ISPRS International Journal of Geo-Information, vol. 7, no. 2, p. 51, 2018.
26. S. Astutik, E. D. Lusiana, N. K. Sa'diyah, R. H. P. Y. Damayanti, F. R. Mashfia, A. Yarcana, F. Y. D. A. S. Saniyawati, U. F. Hidayat, and A. G. B. Octavia, *Bayesian Conditional Autoregressive for Rainfall Modeling in East Java*, Statistics, Optimization & Information Computing, vol. 15, no. 3, pp. 2235–2248, 2026.
27. C. J. Wilmott and K. Matsuura, *Advantages of the mean absolute error (MAE) over the root mean square error (RMSE) in assessing average model performance*, Climate Research, vol. 30, pp. 79–82, 2005.
28. T. Chai and R. R. Draxler, *Root mean square error (RMSE) or mean absolute error (MAE)? – Arguments against avoiding RMSE in the literature*, Geoscientific Model Development, vol. 7, no. 3 pp. 1247–1250, 2014.